Advances in simulations of heat exchange in fluid flows by high-order methods

Jan Pech[1*]

[1]Institute of Thermomechanics of the CAS, Dolejškova 1402/5, 182 00 Praha 8, Czech Republic

Abstract. The article presents high-order simulations of heat transfer in fluid flow. Heat induced changes in material properties (density, viscosity and heat conductivity) substantially influence flow structures. The change of fluid density implies naturally the thermal expansion what results in non-homogeneous divergence of velocity and the model of evolutionary Navier-Stokes-Fourier equations is not strictly incompressible in this case. Proposed algorithm treats the model as a fully coupled system of equations. Applied method of operator splitting is promissing to become a more general concept for numerical modelling of active quantities advected by incompressible fluids. This work follows the 2D results presented during EFM 2019 and extends to 3D together with advances of the code reimplementation to current version of the Nektar++ library (open-source framework for spectral/hp finite elements). Results for various settings for both the forced/mixed and natural convection are shown.

1 Introduction

In this contribution, we are going to revisit the problem of fluid flow coupled with a heat exchange, which was presented in previous EFM conference as a 2D study of natural and forced convection. The algorithm, unless based on the same idea, was reformulated now and implemented as a full 3D solver into the Nektar++ library [1], an open source library supporting the *spectral/hp* finite elements. The solver is expected to be available in the next release of the library. Mentioned 2D studies were based on early version (3.3.0) of Nektar++ and present reimplementation allows combination of new features of the library with the solver, namely stabilisation techniques (spectral vanishing viscosity), algebraic solvers, parallelisation or pre- and post-processing tools.

The set of equations to be discussed is the fully coupled Navier-Stokes-Fourier system with temperature dependent material properties (dynamic viscosity μ, thermal conductivity κ and density ρ).

$$\rho\left(\frac{\partial \mathbf{v}}{\partial t} + \mathbf{v}\cdot\nabla\mathbf{v}\right) = -\nabla p + \frac{1}{\mathrm{Re}}\nabla\cdot(2\mu\mathbb{S}) + \mathrm{Ri}\Theta\mathbf{g} \tag{1a}$$

$$\frac{\partial \rho}{\partial t} + \nabla\cdot(\rho\mathbf{v}) = 0 \tag{1b}$$

$$\rho\left(\frac{\partial T}{\partial t} + \mathbf{v}\cdot\nabla T\right) = \frac{1}{\mathrm{Re}\,\mathrm{Pr}}\nabla\cdot(\kappa\nabla T)\ , \tag{1c}$$

Table 1. Definitions of used nondimensional numbers. Note, that temperature T is normalised by farfield value T^+_∞ instead of widely used characteristic temperature difference ΔT^+.

Name	Symbol	Definition
Prandtl	Pr	$\frac{c^+_{p\infty}\mu^+_\infty}{\kappa^+_\infty}$
Rayleigh	Ra	RiPrRe^2
Reynolds	Re	$\frac{L^+\lvert\mathbf{v}^+_\infty\rvert\rho^+}{\mu^+_\infty}$
Richardson	Ri	$\frac{\Delta\rho^+ g^+ L^+}{\rho^+_\infty\lvert\mathbf{v}^+_\infty\rvert^2}$ or $\frac{g\beta\Delta T L}{\lvert\mathbf{v}_\infty\rvert^2}$

where

$$\mathbb{S} = \mathbb{D} - \frac{1}{3}(\nabla\cdot\mathbf{v})\,\mathbb{I} \tag{2}$$

is related to the deviatoric part of the stress tensor (pure shear stress) and $\mathbb{D} = \frac{1}{2}\left[\nabla\mathbf{v} + (\nabla\mathbf{v})^{\mathrm{T}}\right]$. This dimensionless system of equations represents a model for flow of a heated fluid, while the fluid is supposed to be Newtonian, calorically perfect and obeying Fourier's law of heat conduction. The unknowns are velocity $\mathbf{v} = (u, v, w)^{\mathrm{T}}$, pressure p and temperature T, other symbols are listed in table of nomenclature. Used dimensionless numbers are summarized in table 1.

* Corresponding author: jpech@it.cas.cz

Nomenclature

(We use dimensionless formulation, if a quantity acts as with physical units it is denoted by superscript "$^+$")

a, $\mathbf{a}$, $\mathbb{A}$	scalar, vector, tensor	*Greek letters*	
c_p^+	specific heat at constant pressure	β	thermal expansion coefficient
g^+	gravitational acceleration	κ	thermal conductivity
$\mathbf{g}$	unit vector in direction of gravitational force	μ	dynamic viscosity
$\mathbb{I}$	unit tensor	ρ	density
L^+	characteristic length	Ω	computational domain
$\mathbf{n}$	unit normal vector to a boundary		
p	pressure	*Symbols*	
t	time	$\lvert\cdot\rvert$	vector magnitude
T	temperature $T = \frac{T^+}{T^+_\infty}$, $T_r = \frac{T^+_W}{T^+_\infty}$	$(\cdot)^{\mathrm{T}}$	transposition
Θ	temperature $\Theta = \frac{T^+ - T^+_\infty}{T^+_W - T^+_\infty}$	∇, $\nabla\cdot$, $\nabla\times$	gradient, divergence, curl
$\mathbf{v} = (u, v, w)$	velocity	∇^2	Laplace

Presented system considers the velocity to be divergent as a consequence of the thermal expansion unless the model originates in the incompressible formulation. This ambiguity follows from dependence of density purely on temperature, while the dependence on pressure is neglected. The system and algorithm get close to the border between incompressible and compressible formulations. Especially between numerical methods for incompressible and compressible flow have been substantial differences.

2 Algorithm

Proposed algorithm is derived from the high-order splitting scheme introduced for the incompressible Navier-Stokes system in Karniadakis [2] and splitting approach for variable viscosity of Karamanos [3]. Main aspects of its derivation stays in approximation of the time derivatives by Backward Difference formulas (BDF) and splitting the system to implicitly solved pressure-Poisson equation and a second order problems of form $(\nabla^2 - \lambda)u = f$. Idea for incorporating a time dependent material property (q) stays in its representation in form $q(\mathbf{x}, t) = \bar{q} + q_s$, where $\bar{q}$ is a time-independent part (constant or generally $\bar{q} = \bar{q}(\mathbf{x})$) scaling the implicitly treated operators, while $q_s = q_s(\mathbf{x}, t)$ acts in time-dependent terms evaluated within extrapolation (see Pech [4]). It is worthy to note, that we do not impose any restriction to the form of the functions describing temperature dependencies of material properties, they are expected to be fully nonlinear. The algorithm solves each step at once without any iterative process.

Its detail description is beyond the scope of this article. Denoting extrapolation of Q-th order

$$[u]^* = \sum_{q=0}^{Q} u_{n-q} \approx u_{n+1}$$

and BDF

$$\left[\frac{\partial u}{\partial t}\right]^{BDF}_{n+1} = \frac{\gamma u_{n+1} - \sum_{q=0}^{Q} \alpha_q u_{n-q}}{\Delta t} \approx \left.\frac{\partial u}{\partial t}\right|_{n+1},$$

the main steps may be sketched as follows:

1. Pressure-Poisson equation

$$\nabla^2 p = \frac{\gamma}{\Delta t}\left[\left[\frac{\partial \rho}{\partial t}\right]^{BDF}\right]^* + \nabla\cdot\left\{\frac{\gamma}{\Delta t}\rho^* \sum_{q=0}^{Q-1}\frac{\alpha_q}{\gamma}\mathbf{v}_{n-q} + [\mathcal{A}]^*\right\} \quad (3)$$

   supplemented by the *High Order Pressure Boundary Condition* (HOPBC)

$$\frac{\partial p}{\partial \mathbf{n}} = \mathbf{n}\cdot\left[\quad -\rho_n\left[\frac{\partial \mathbf{v}}{\partial t}\right]^{BDF}_n + \mathcal{A}\right]^* \quad (4)$$

2. elliptic problem for each of the velocity components

$$\nabla^2 \mathbf{v}_{n+1} - \frac{\gamma \mathrm{Re}}{\Delta t}\mathbf{v}_{n+1} = \mathcal{F}_{\mathcal{V}}([\mathcal{A}]^*, [\nabla d - \nabla\times\nabla\times\mathbf{v}]^*). \quad (5)$$

3. the same type of elliptic equation, with specific source term, is solved finally for temperature

$$\left(\nabla^2 - \mathrm{RePr}\frac{\gamma}{\Delta t}\right)T_{n+1} = \ldots \quad (6)$$

where

$$\mathcal{A} = -\rho(\mathbf{v}\cdot\nabla\mathbf{v}) + \frac{1}{\mathrm{Re}}\left(-\mu\nabla\times\nabla\times\mathbf{v} + \nabla\mu\cdot\left[\nabla\mathbf{v} + (\nabla\mathbf{v})^{\mathrm{T}}\right] - \frac{2}{3}(\nabla\mu)\, d + \frac{4}{3}\mu\nabla d\right) + \mathbf{f}^{EX}. \quad (7)$$

and divergence is evaluated as

$$d = -\frac{1}{\rho}\left(\left[\frac{\partial \rho}{\partial t}\right]^{BDF} + \mathbf{v}\cdot\nabla\rho\right). \quad (8)$$

The correctness of the algorithm implementation and its convergence properties were tested using a smooth and bounded manufactured solution. For illustration, x-velocity component of the used exact solution was `u =2.0*cos(PI*x)*cos(PI*y)*cos(PI*z)*sin(t)`,

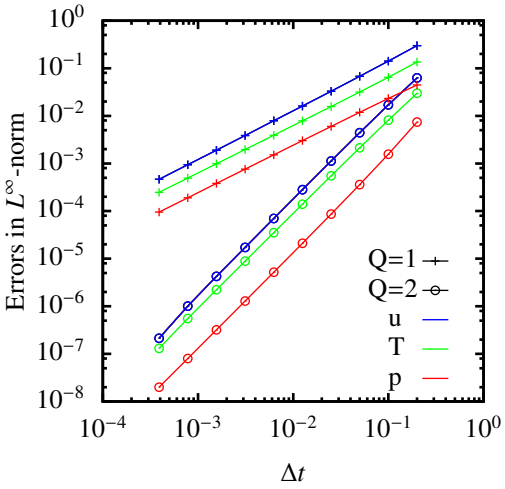

Fig. 1. First and second order, $Q = 1, 2$, convergence in time $\Delta t \to 0$.

other velocity components, temperature and pressure were in similar form. Functions describing temperature dependencies of material were set to identical form of power law $\rho = \mu = \kappa = (1 + 0.1T)^2$ for the convergence test. Error decay in u, T and p with shortening the timestep Δt is shown in L_∞-norm in fig. 2. Polynomial degree for this test was set to 14, sufficient for full resolution in spatial coordinates. Presented error decay therefore completely belongs to discretisation in time. Figure 2 shows the error decay of the scheme if the Dirichlet boundary condition is imposed, convergence with full HOPBC is slower in pressure component due to the error arising from boundary extrapolation and the fact, that pressure-Poisson step becomes fully Neumann.

The new implementation of the solver was applied in simulations of natural convection and forced convection/transient flow, studied previously using the same method in 2D.

3 Simulations

The temperature dependencies of material properties require knowledge of the farfield thermodynamic state. However, this information is often missing in published results. Materials have different properties at different temperatures and not only in their values, but also in sense of derivatives. Knowledge of values is sufficient for evaluation of the dimensionless numbers, but derivatives play an important role in our model and are unknown if the thermodynamic state of the experiment is not specified. Unfortunately, information about T_∞ was not found in none of the paper we followed (Kuehn [5], Ren [6]). For that reason, $T_\infty = 293, 15$ was set, but it might be an artificial source of inaccuracy.

To check the scheme performance on a wider variety of cases, parameters for air were set in case of natural convection, while water flow was studied in case of transient

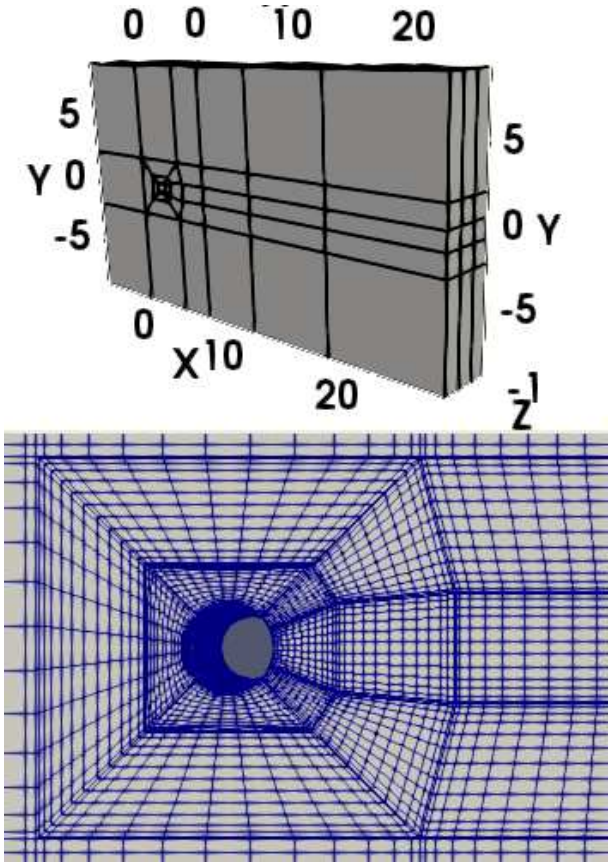

Fig. 2. Top: Computational mesh consisting of 111 elements. Bottom: Detail to cylinder area, abscissas connect the integration poins.

convection (in case of constant properties, models would be indistinguishable). The dependencies followed from fitting the data tabulated in [7] resulting as power laws or second order polynomial approximations.

Computational domain Ω for both tests was chosen to be of the same spatial extent 23x18x4 (cylinder diameter $L = 1$), the same as used in Ren [6]. Curved boundary of the cylinder was approximated by polynomial of order 15, which is sufficient for full resolution of this curvature. In both regimes the mesh consisting of 111 elements was used, see Fig. 3. Such a low number of elements in the mesh brings a limit for the number of cores over which the task may be parallelised.

3.1 Natural convection

Study of the natural convection was inspired by existence of data from Kuehn [5], which were already used for comparison with results obtained with the 2D Navier-Stokes-Fourier solver. The data are two dimensional, but geometrical setting of our 3D model is not expected to induce 3D patterns in vicinity of the source of heat.

The farfield/reference temperature was chosen to be $T_\infty = 293.15$, and ratio $T_r = \frac{T\_W}{T_\infty} = 1.01$ (T_W is the temperature of cylinder wall). Material parameters refered to air, therefore Pr $= 0.71$. The Reynolds number was set

Table 2. Boundary conditions used in the natural convection simulation. All the Neumann boundary conditions denoted $\frac{\partial \bullet}{\partial \mathbf{n}}$ were homogeneous, "HOPBC" denotes 4.

	$\mathbf{v}$	T	p
inflow	$(\frac{\partial u}{\partial \mathbf{n}}, \frac{\partial v}{\partial \mathbf{n}}, 0)$	1	0
top&bottom	$\left(\frac{\partial u}{\partial \mathbf{n}}, 0, \frac{\partial w}{\partial \mathbf{n}}\right)$	$\frac{\partial T}{\partial \mathbf{n}}$	HOPBC
outflow	$\left(\frac{\partial u}{\partial \mathbf{n}}, \frac{\partial v}{\partial \mathbf{n}}, \frac{\partial w}{\partial \mathbf{n}}\right)$	$\frac{\partial T}{\partial \mathbf{n}}$	0
cylinder	$(0, 0, 0)$	T_r	HOPBC
front&back	$\left(\frac{\partial u}{\partial \mathbf{n}}, \frac{\partial v}{\partial \mathbf{n}}, 0\right)$	$\frac{\partial T}{\partial \mathbf{n}}$	HOPBC

Table 3. Overview of boundary conditions used in the transient flow simulation. All the Neumann boundary conditions denoted $\frac{\partial \bullet}{\partial \mathbf{n}}$ were homogeneous, "HOPBC" denotes 4.

	$\mathbf{v}$	T	p
inflow	$(1, 0, 0)$	1	HOPBC
top&bottom	$\left(\frac{\partial u}{\partial \mathbf{n}}, 0, \frac{\partial w}{\partial \mathbf{n}}\right)$	$\frac{\partial T}{\partial \mathbf{n}}$	$\frac{\partial p}{\partial \mathbf{n}}$
outflow	$\left(\frac{\partial u}{\partial \mathbf{n}}, \frac{\partial v}{\partial \mathbf{n}}, \frac{\partial w}{\partial \mathbf{n}}\right)$	$\frac{\partial T}{\partial \mathbf{n}}$	0
cylinder	$(0, 0, 0)$	T_r	HOPBC
front&back	$\left(\frac{\partial u}{\partial \mathbf{n}}, \frac{\partial v}{\partial \mathbf{n}}, 0\right)$	$\frac{\partial T}{\partial \mathbf{n}}$	$\frac{\partial p}{\partial \mathbf{n}}$

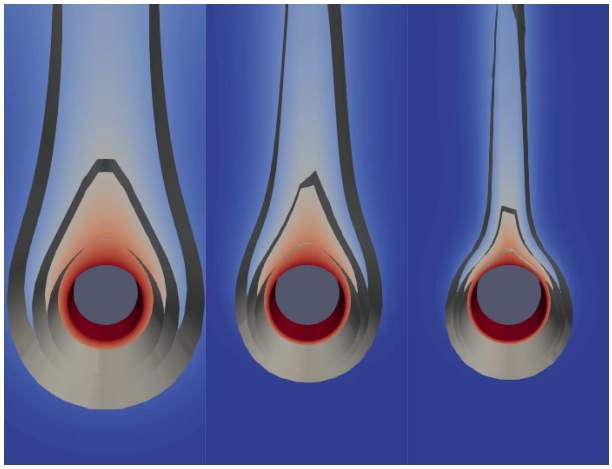

Fig. 3. Comparison of temperature distribution in vicinity of heated cylinder for Ra = 100 (left), Ra = 10^3 (center) and Ra = 10^4 (right).

to Re = 120. Computation was performed with timestep $\Delta = 0.005$ and polynomial approximation in spatial coordinates was of degree 10. Setting of the boundary conditions is summarized in table 3.1.

Only very basic outflow condition was available for the newly implemented solver and size of the computational domain was limited what resulted in instability of the computation at the time, when the wake structures touched the "outflow" boundary. However, the domain extent was sufficient to allow development of the field around the cylinder, see Fig. 3.1.

Contours of temperature in this buoyancy driven flow well coincide with results obtained for the same Rayleigh numbers in mentioned 2D simulations. More detail studies of 3D structures emerging later downstream are left for a future investigations.

3.2 Transient flow

The second simulation was an attempt to reconstruct results published in Ren[6] using currently implemented algorithm, which extends substantially the model (previous results were taken strictly with constant parameters and homogeneous divergence).

Boundary conditions set in this case are summarized in table 3.2, $T_r = 1.01$.

The flow at Re = 85 and Ri = 1.0 stayed in the regime of parralel vortex shedding for very long time in current simulations, unless it is known it is unstable also in the spanwise direction. This may be a consequence of low level of numerical noise produced in spatial coordinates if high order approximation is used. Similar observation was reported also in 2D study comparing spectral/hp element method with the finite volumes in [8]. Therefore we imposed a small disturbance to velocity field in z-coordinate to speed up development of the final structures. Studied flow regime did not dump this impuls and slowly developed. In time interval $t \in [330 : 380]$ we can observe periodic evolution of the fluid forces acting to the cylinder, Fig. 3.2.

Accordingly to periodicity and amplitude in evolution of the aerodynamic forces (Fig. 3.2) we deduce, that the flow was fully developed after 350 time units. Periodic variation of small amplitude was observed also in the spanwise direction of velocity.

The final part of the simulations was done with polynomial degree 13 (in each spatial direction) and time step $\Delta t = 0.005$. Computation was parallelized up to 48 cores. Final part, where the full resolution was used, $t \in [300 : 380]$ (15000 steps), then took approx. 12000 s. To solve the global algebraic system, direct parallel XX^T solver with multilevel static condensation was used. Therefore a significant time interval of the computation was covered by evaluation of the inverse system, approx 1/4 of the computational time.

Unless the simulations were not pushed to extreme accuracy which high order methods offer, obtained results very well resemble structures described in Ren [6]. The three-dimensional structures, Fig. 3.2 are qualitatively comparable with [6] (pg. 28, fig. 2.13.). In Fig. 3.2, it is observable, that the pattern in y-component of vortic-

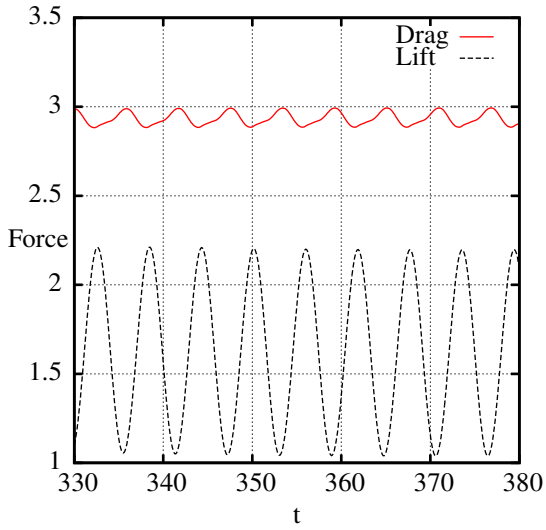

Fig. 4. Time evolution of drag and lift force for mixed convection case (Re = 85, Ri = 1.0).

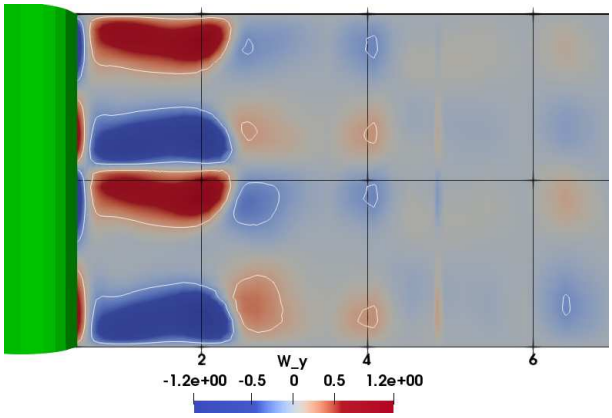

Fig. 5. Re = 85, Ri = 1.0, y-component of vorticity ω_y at $y = 0$.

ity is not positioned symmetrically at the presented time. This coincides with periodical evolution of low amplitude in mentioned spanwise component of force acting onto the cylinder.

Achieved data were processed at the same contour levels as in work of Ren [6]. Figure 3.2 shows contours of temperature and vorticity in x-direction. The polynomial space used in this simulation seems to be sufficient to represent tiny structures both in temperature and velocity in the wake behind the heated cylinder.

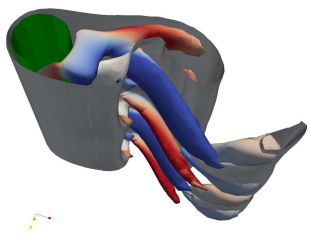

Fig. 6. Re = 85, Ri = 1.0, x-component of vorticity ω_x, contours at ±0.4 and temperature isosurface at $T = 1.0015$.

4 Conclusion

The main achievement presented in this contribution is in successful implementation of original scheme, which is suitable for simulations based on spectral/hp element method. The algorithm was implemented into the most current version of the open-source library Nektar++ and is supposed to be included in a next release version.

Present study showed, that the algorithm achieves expected convergence orders in time and is applicable to simulations of real physical processes.

Acknowledgements. The author wishes to acknowledge the support of the Czech Academy of Sciences, project MSM100761901.

References

[1] C. Cantwell, D. Moxey, A. Comerford, A. Bolis, G. Rocco, G. Mengaldo, D.D. Grazia, S. Yakovlev, J.E. Lombard, D. Ekelschot et al., Computer Physics Communications **192**, 205 (2015)

[2] G.E. Karniadakis, M. Israeli, S.A. Orszag, Journal of Computational Physics **97**, 414 (1991)

[3] G.S. Karamanos, S. Sherwin, Applied Numerical Mathematics **33**, 455 (2000)

[4] J. Pech, *Scheme for Evolutionary Navier-Stokes-Fourier System with Temperature Dependent Material Properties Based on Spectral/hp Elements*, in *Spectral and High Order Methods for Partial Differential Equations ICOSAHOM 2018*, edited by S.J. Sherwin, D. Moxey, J. Peiró, P.E. Vincent, C. Schwab (Springer International Publishing, Cham, 2020), pp. 465–475, ISBN 978-3-030-39647-3

[5] T. Kuehn, R. Goldstein, International Journal of Heat and Mass Transfer **23**, 971 (1980)

[6] M. Ren, Ph.D. thesis, Mechanical Engineering (2005)

[7] B. Gebhart, *Heat Conduction and Mass Diffusion*, McGraw-Hill series in mechanical engineering (McGraw-Hill, 1993), ISBN 9780071125147

[8] J. Pech, P. Louda, *Comparison of Finite Volume and Spectral/HP Methods on Navier - Stokes Equations for Unsteady Incompressible Flow*, in *Proceedings Topical Problems of Fluid Mechanics 2018* (2018), pp. 223–230